Localized characterization of charge transport and random telegraph noise at the nanoscale in HfO$_2$ films combining scanning tunneling microscopy and multi-scale simulations

R. Thamankar, F. M. Puglisi, A. Ranjan, N. Raghavan, K. Shubhakar, J. Molina, L. Larcher, A. Padovani, P. Pavan, S. J. O'Shea, and K. L. Pey

---

Localized characterization of charge transport and random telegraph noise at the nanoscale in HfO$_2$ films combining scanning tunneling microscopy and multi-scale simulations

R. Thamankar,[1,2,a)] F. M. Puglisi,[3,a)] A. Ranjan,[1] N. Raghavan,[1] K. Shubhakar,[1] J. Molina,[4] L. Larcher,[5,6] A. Padovani,[6] P. Pavan,[3] S. J. O'Shea,[7] and K. L. Pey[1]

[1]*Singapore University of Technology and Design, 8 Somapah Road, 487372 Singapore*
[2]*School of Advanced Sciences, VIT University, Vellore, Tamil Nadu 632014, India*
[3]*DIEF, Università di Modena e Reggio Emilia, Via P. Vivarelli 10/1, Modena 41125, Italy*
[4]*National Institute of Astrophysics, Optics and Electronics, Tonantzintla, Puebla, Mexico*
[5]*DISMI–Università di Modena e Reggio Emilia, Via Amendola 2, Reggio Emilia 42122, Italy*
[6]*MDLab s.r.l. - Località Grand Chemin 30, Saint-Christophe, Aosta 11020, Italy*
[7]*Institute of Materials Research and Engineering (IMRE), A*STAR, 2 Fusionopolis Way, Singapore 138634*

Charge transport and Random Telegraph Noise (RTN) are measured successfully at the nanoscale on a thin polycrystalline HfO$_2$ film using room temperature Scanning Tunneling Microscopy (STM). STM is used to scan the surface of the sample with the aim of identifying grains and grain boundaries, which show different charge transport characteristics. The defects responsible for charge transport in grains and grain boundaries are identified as positively charged oxygen vacancies by matching the localized *I-V* curves measured at the nanoscale with the predictions of physics-based multi-scale simulations. The estimated defect densities at grains and grain boundaries agree with earlier reports in the literature. Furthermore, the current-time traces acquired by STM at fixed bias voltages on grains show characteristic RTN fluctuations. The high spatial resolution of the STM-based RTN measurement allows us to detect fluctuations related to individual defects that typically cannot be resolved by the conventional device-level probe station measurement. The same physical framework employed to reproduce the *I-V* conduction characteristics at the grains also successfully simulates the RTN detected at the nanoscale. We confirm that charge trapping at defects not directly involved in charge transport can induce significant current fluctuations through Coulombic interactions with other defects in the proximity that support charge transport. *Published by AIP Publishing.* [http://dx.doi.org/10.1063/1.4991002]

I. INTRODUCTION

In recent years, metal oxides have found increasing importance in the field of nanoelectronics. Particularly, HfO$_2$ is widening its application in the semiconductor industry, representing the preferred high-κ gate dielectric in sub-45 nm CMOS nodes[1] and being currently investigated as a switching layer in advanced non-volatile memory concepts such as resistive random access memory (resistive switching) devices (ReRAMs).[2] However, in spite of its compatibility with the CMOS process, HfO$_2$ intrinsically contains a higher bulk defect density and a poorer interface with Si, as compared to SiO$_2$ (native oxide of silicon).[3] This calls for in-depth study of several critical issues in HfO$_2$-based devices such as gate leakage current,[4] positive and negative bias temperature instability,[5,6] random telegraph noise (RTN),[7] and soft/hard dielectric breakdown.[8] In the last decade, considerable research efforts brought about important experimental evidence about the role of defects in each of these phenomena.[9] Although the physical mechanisms governing charge transport and related phenomena through HfO$_2$ stacks are still widely debated, there is a consensus about oxygen vacancy defects being the main cause for leakage current,

stochastic degradation, and eventual failure of HfO$_2$ gate dielectrics at low bias voltages.[10,11] Moreover, besides contributing to a significant component of the overall leakage current, structural defects are supposedly involved in the low-frequency noise phenomena, which is gaining even more significance as device size continues to shrink.[12] Low-frequency signals typically appear in a form of random telegraph noise (RTN),[13] which displays abrupt and random fluctuations of current among the discrete number of conduction levels. The analysis of the RTN characteristics can be useful to identify the nature of the defects responsible for the RTN phenomenon. A popular approach to study the defect dynamics is to perform RTN analysis at the device level, which is assumed to result from the stochastic capture/emission of charge carriers at defect sites.[13] The downside of these device-level measurements is that the RTN signatures tend to be hidden within the white noise and *1/f* noise components that arise from the leakage through the bulk defects/traps, especially in relatively large devices (from around 100 nm to several microns in unit dimension). As a result, accurate analysis of RTN in nanoscale devices is a challenge, and individual defect/trap responsible for RTN trends could be observed only when the oxide has degraded sufficiently, e.g., when it suffers a percolation breakdown.[14] In order to determine the properties of the traps and their dynamics at

---

a)R. Thamankar and F. M. Puglisi contributed equally to this work.

the nanoscale, probing a few or individual defects by suitable characterization techniques with high spatial resolution is extremely important. In this context, scanning tunneling microscopy (STM) and conductive atomic force microscopy (cAFM) may be preferential choices to characterize defects at the nanoscale.[15–19] STM is commonly employed to study pure electronically conducting materials such as Nb-doped SrTiO$_3$, or materials with mixed conductivity like Cu$_2$S, and Ag$_2$S,[20–22] while it is rarely used to study the high-κ dielectric materials at the nanoscale.[15] Recently, the STM-tip induced resistive switching in TaO$_x$, HfO$_x$, and TiO$_x$ thin films has also been reported.[23–25]

In this work, we report the results of a study on charge transport and RTN of a HfO$_2$ thin film on Si(100) using a room temperature STM operating under ultra-high vacuum (UHV) ($\sim 5 \times 10^{-10}$ mbar). We address the nature of electrically active defects in HfO$_2$ by focusing on the process-induced defects located within the HfO$_2$ film. In order to understand the mechanisms responsible for charge transport and its alterations (i.e., RTN), we combine specific STM investigations with multi-scale simulations. Particularly, we will

i)   identify suitable locations for RTN measurements by recognizing grains and grain boundaries (GB) using topography and conductivity mapping using STM;

ii)   perform spatially localized *I-V* measurements of grains and grain boundaries;

iii)   identify the defects contributing to the current and the dynamics of defect generation leading to the breakdown;

iv)   perform spatially localized RTN measurements on suitable locations; and

v)   identify the possible atomic configurations responsible for the observed RTN.

In this respect, this work presents several innovations: the nano-scale defect characterization of HfO$_2$ films is indeed seldom performed with the precise, non-invasive STM tool and provides far more detailed information at the atomic (single defect) level than the traditional characterization techniques at the device level. Furthermore, this is the first time to the authors' knowledge that charge transport, breakdown, and RTN are self-consistently measured at the nanoscale and interpreted using a unique comprehensive multi-scale simulation framework, thereby providing a unified picture (validated at the nanoscale) of the role of defects in these thin films. The main advances of this contribution lie indeed in the powerful combination of spatially localized STM investigation with sophisticated multi-scale simulations, resulting in an unprecedented detailed understanding of charge transport, breakdown kinetics, and RTN. The results shown in this contribution allow us to probe the kinetic behavior of a single oxygen vacancy defect and examine the impact of the dielectric microstructure on the intrinsic physics of degradation and failure in high-κ gate stacks in MOSFET and FinFET devices (without the interference of any oxygen scavenging metal electrode). In addition, they can provide unique insights into the process of filament formation in HfO$_2$-based resistive memories.[2,9–11]

II. DEVICES, EXPERIMENTS, AND SIMULATIONS

Our sample consists of a ~ 4 nm HfO$_2$ film deposited on n-Si(100) using the atomic layer deposition (ALD) technique with H$_2$O and Tetrakis(dimethylamino) hafnium (TDMAH) as precursors at 250 °C. The sample was then annealed at 400 °C for 40 min in an N$_2$ ambient, which resulted in a polycrystalline HfO$_2$ film.[15] The absence of a top metal electrode allowed us to directly analyze the dielectric layer excluding any possible interaction between the oxide and the metal layer, typically occurring at their interface during annealing. These interactions can be detrimental resulting in local structural modification of the oxide, e.g., the oxygen scavenging action of the top metal electrode during annealing could induce graded sub-stoichiometry in the HfO$_2$ layer.[26]

Experiments were conducted at room temperature using an ultrahigh vacuum scanning tunneling microscope (UHV-STM, $p \sim 5 \times 10^{-10}$ mbar) with a Pt-Ir tip, which allowed a localized study of the HfO$_2$ film with a lateral spatial resolution as low as ~ 10 nm.[15] Since the sample has no metal electrode on top of the HfO$_2$ layer, the STM tip itself acted as a non-invasive local electrode when placed sufficiently close to the sample surface to meet tunneling conditions. The actual structure under investigation consists of (i) a *n*-Si layer; (ii) a HfO$_2$ layer; (iii) a vacuum tunnel layer; and (iv) a Pt-Ir metal tip of the STM. Hence, the bias voltage applied (V_{bias}) drops across three junctions/layers, namely, the vacuum tunnel junction (V_{vac}), the high-κ dielectric (V_{hk}), and the *n*-Si (V_{Si}) (ignoring the presence of any interfacial SiO$_x$ layer). The thickness of the vacuum tunnel junction is estimated by measuring the dependence of the tunneling current on the physical separation from the sample. We have measured such a dependence of tunnel current with separation in our previous work, obtaining $t_{vac} \approx 0.7$ nm (which represents the distance and control conditions for tunneling current in the fabricated sample).[15]

Initially, the sample was scanned to identify grains and grain boundary contours on the top surface. The tip was biased at 3.5 V and its height was repeatedly adjusted as the tip moved over the sample surface to maintain a constant current value, typically ~ 50 pA. In addition, a lock-in feedback system allowed superimposing a fixed-frequency AC voltage signal to the DC tip bias. This scanning mode allows simultaneously acquiring the topographic image and the conductivity map (dI/dV) of the polycrystalline HfO$_2$ film, as shown in Figs. 1(a) and 1(b), respectively. The results show the different conductivity regions across the whole sample surface, i.e., grains (G) and grain boundaries (GB). To correlate the two images, a line scan was taken across the two images and plotted, as shown in Fig. 1(c). The black and red lines refer to the topography and the dI/dV maps, respectively. The "crests" on the topography line scan (black curve) correspond to the grains showing lower conductivity (red curve) as shown by the lower dI/dV signal in those areas. This is a clear evidence to show that the HfO$_2$ grains have lower conductivity compared to the grain boundaries, in agreement with the earlier reports.[27] The dI/dV maps were taken as a reference to place the STM tip precisely on the HfO$_2$ grains and grain boundaries to perform the localized
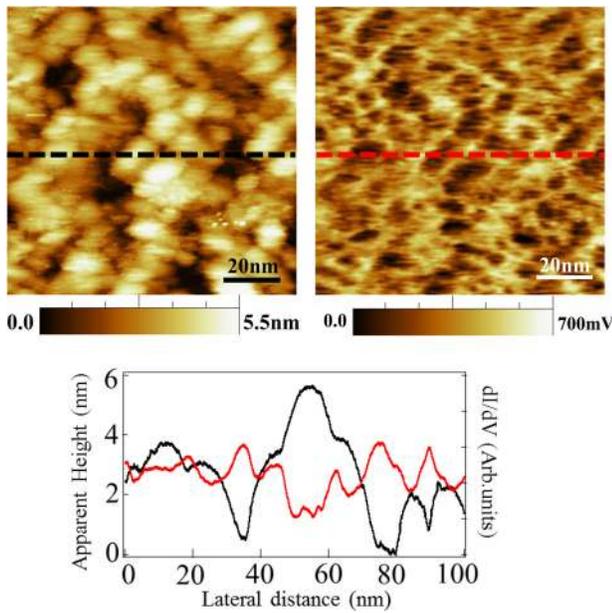
FIG. 1. A typical topographical image of the HfO$_2$ thin film is shown in (a). The corresponding dI/dV image is shown in (b). Scanning parameters: 3.5 V/ 50 pA. Area: 100 nm × 100 nm. Lock-in parameters: 2.7 kHz/10mV$_{ac}$. The bright regions in the topographic image correspond to the dark regions (lower conductivity) in the dI/dV map. For clarity, a z-scale on both the figures is shown. For a comparison, line scans are drawn on both the topographic image (black dotted line) and the dI/dV map (red dotted line), as shown in (c).

study of charge transport and RTN properties. The charge transport study was performed by positioning the tip on either grains or grain boundaries and then applying a voltage ramp (from 0 V to 6 V, with a ramp rate of $dV/dt = 1$ V/s) to the tip. Similarly, localized RTN measurements were performed by positioning the tip on unstressed grains (i.e., locations at which a lower defect density is estimated) and applying a constant voltage to the tip while sampling the current over time with a sampling time interval of $\tau_s = 100$ μs. To increase the chances of measuring the RTN signal related to an individual process-induced defect, it is required to select a low defect density location (i.e., a grain). To minimize the amount of stress delivered to the localized area of interest, the current-time measurements were done for a very short duration, spanning a few tens of seconds. Specifically, we select the appropriate voltage range for RTN

measurements (i.e., V_{bias} ranging from 3.4 V to 4.0 V) to minimize the defect generation (activation) probability (note that only a fraction of V_{bias} drops across the HfO$_2$ layer). Moreover, the short duration of the measurements also avoids the thermal drift of the STM tip.[15]

To understand the physics in the governing processes occurring during the RTN measurements, the measured RTN signals were fitted with simulations performed using the MDLab® package.[28] This tool allows connecting the microscopic properties of the materials to the macroscopic electrical device performance trends in a generalized multi-scale simulation framework as shown in Fig. 2, where material imperfections and non-idealities (e.g., vacancies, ions) are also accounted for. Many different charge transport processes (e.g., drift, diffusion, direct and Fowler-Nordheim tunneling, thermal emission, trap-assisted tunneling (TAT), etc.) are simultaneously considered. The interaction between tunneling electrons/holes and atomic defects (originated at broken atomic bonds) were modeled in the framework of the multi-phonon TAT model, where the electron/hole–phonon coupling and the atomic lattice relaxation occurring due to charge trapping and emission are included through the multi-phonon transition probability.[29] The average capture and emission times of electrons and holes are self-consistently calculated for each defect, considering all the possible capture and emission processes (which also includes the possible charge transition among different defects). These characteristic trap-assisted tunneling (TAT) rates depend strongly on the local values of temperature and electric field, as well as on the intrinsic properties of the defect species considered, (i.e., the thermal ionization and relaxation energies of the atomic species). These are typically calculated using *ab–initio* techniques. Importantly, it is possible to introduce many different layers of different materials, whose properties and morphology are considered.[29–31] These features allow a precise definition of the structure of the device to be simulated, including all the relevant processes encompassing charge transport. Moreover, structural modification possibly occurring in the device as a result of external stress must be considered as well. Particularly, the processes of generation and recombination of the atomic species (ions, vacancies, and interstitials) are also self-consistently included as shown in Fig. 2. For every point in space and time, the defect
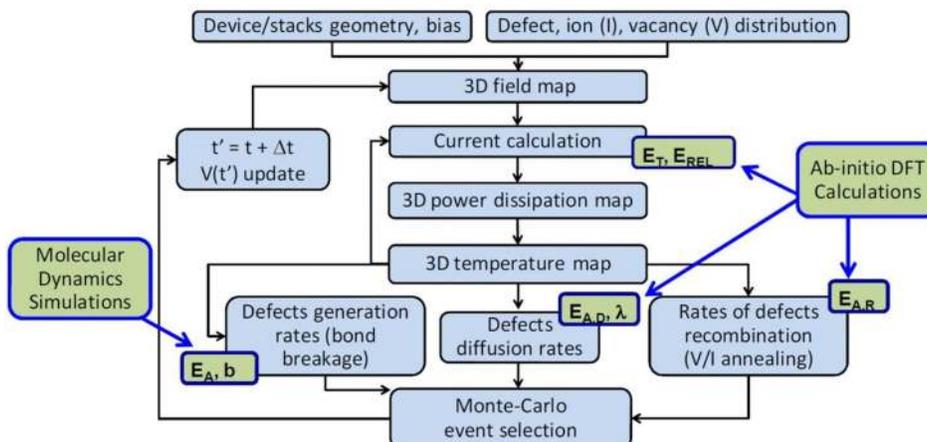
FIG. 2. Schematic illustration of the multi-scale simulation framework. The interactions between electrons/holes and atomic species, together with their dependence on external conditions (field, temperature), device structure, material properties, and morphology are included. A multi-scale approach is used to include the different mechanisms simultaneously occurring in the simulated structure. The parameters defining the defects/atomic species properties are taken from *ab-initio* DFT and molecular dynamics simulations.

generation and recombination rates are calculated considering their dependence on the local electric field (in turn influenced by fixed and trapped charges) and the temperature (influenced by the local power dissipation) in the framework of the McPherson's thermo-chemical bond breakage model.[32] This model allows the calculation of the rate of bond breakage and defect pair generation at any location in the device. Similarly, the defects' diffusion rates are calculated once the local electric field and temperature information is available. The activation energies for defect diffusion are taken from the literature and typically calculated by means of molecular dynamics simulations that are able to consider the differences in local morphology and chemical arrangements. The 3D temperature and potential maps, necessary to properly calculate capture/emission times, and generation/recombination/diffusion rates are calculated by solving the Fourier heat equation (which includes the contribution of the power dissipated at localized defects supporting charge transport) and the Poisson equation (which is solved including fixed and trapped charges). At each simulation step, the calculated capture/emission times and generation/recombination/diffusion rates are fed into a Monte-Carlo (MC) engine that randomly selects which process should happen based on the aforementioned probabilities. This software, which allows performing full 3D simulations of the device,

was used to reproduce the experimental *I-V* curves acquired on individual grains and grain boundaries. Simulations of the current-time traces could be performed as well by using the built-in kinetic Monte-Carlo (kMC) module. Further details about the simulation environment may be found in Ref. 28. The structure used in the simulations in this work consists of an *n*-Si layer, a 4 nm HfO$_2$ layer, a 0.7 nm thick vacuum layer, and a Pt-Ir metal layer, which mimics the presence of the Pt-Ir STM tip. The cross-section of the simulated sample is $10 \times 10 \, nm^2$, which roughly corresponds to the estimated scanning area of the Pt-Ir tip under optimum tunneling conditions. In this respect, the extreme spatial resolution of STM measurements allows simulating the entire 3D volume under investigation in a reasonable amount of time, which is a clear advantage over device level studies.

III. RESULTS AND DISCUSSION

A. Charge transport at grain and grain boundaries

The results of the *I-V* investigation conducted on several grain and grain boundary sites are shown in Fig. 3. Despite some intrinsic site-to-site material variability, it can be clearly seen that the currents measured at the GB sites [Fig. 3(b)] are significantly higher than those measured at the grains [Fig. 3(a)] in the voltage range between 3 and 5 V.
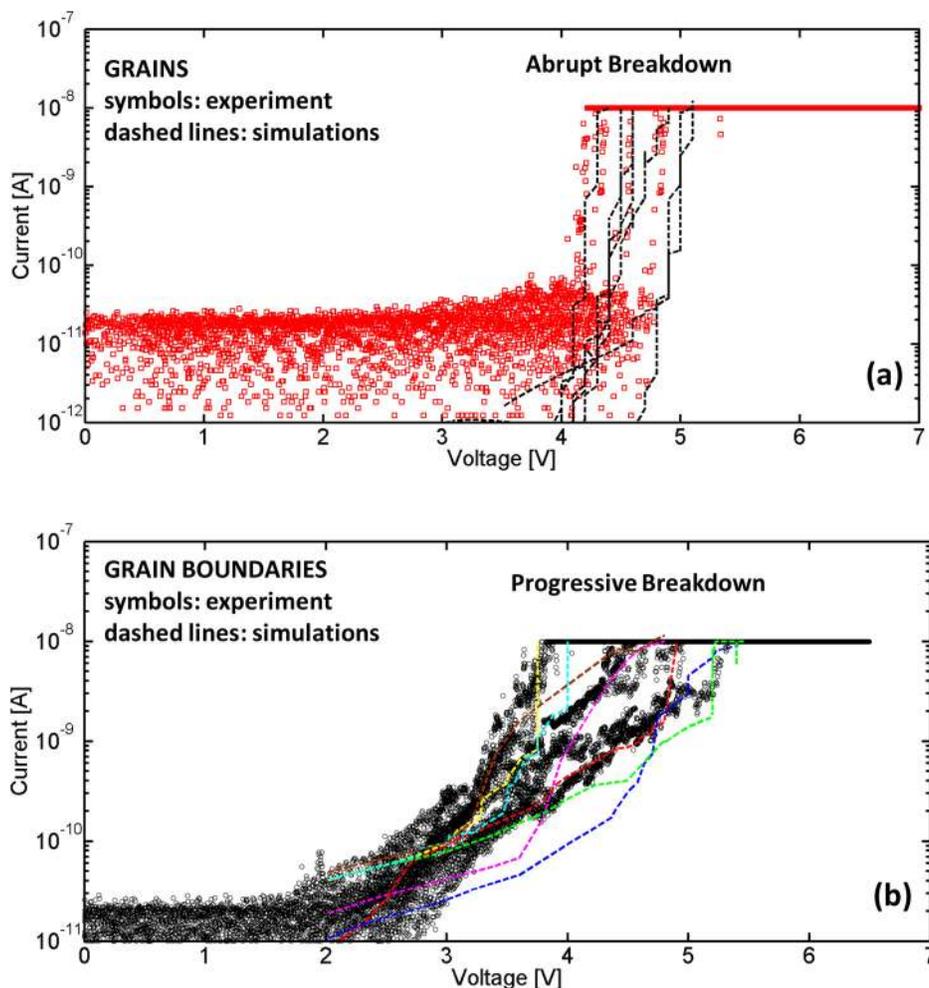
FIG. 3. *I-V* breakdown characteristics on (a) grains and (b) grain boundaries. Both the experimental data (symbols) and the simulations results (dashed lines) are plotted in the same graph for comparison. The current-voltage characteristics recorded on grains show an abrupt breakdown (a), correctly reproduced by simulations (dashed lines). The current-voltage characteristics at the grain boundaries show completely different characteristics with a progressive breakdown (b). The dotted lines represent the results of computations performed by considering a $10 \times 10 \, nm^2$ structure, which approximately reproduces the experimental trends (black symbols).

Particularly, the current measured on grains was usually below the background noise level of the measurement setup (i.e., 10 pA) for voltages up to about 4 V and abruptly increased when breakdown occurred. Conversely, the *I-V* curves measured on the grain boundaries were characterized by higher current values at low voltages and showed a progressive degradation, culminating in the breakdown. These results are consistent with the previous observations performed with cAFM[33,34] and confirm that the grain boundaries in the polycrystalline HfO$_2$ films represent the preferential paths for charge transport. In recent years, the combination of *ab–initio* calculations and device-level experimental results has suggested that the charge transport through the poly-crystalline HfO$_2$ occurs primarily through trap-assisted tunneling of charge carriers assisted by positively charged oxygen vacancies, which tend to thermodynamically segregate at the grain boundaries.[35] This suggests that grains and grain boundaries are associated with different densities of process-induced defects, with grain boundaries constituting highly oxygen-deficient and sub-stoichiometric regions. The defect densities considered in the simulations to match the experimental *I-V* curves for grains and grain boundaries are $3–5 \times 10^{19}$ cm^{-3} and $7–9 \times 10^{20}$ cm^{-3}, respectively, in agreement with previous studies.[15] Nevertheless, for the sake of completeness, simulations also consider the contributions of different charge transport mechanisms, (i.e., Fowler-Nordheim, direct tunneling, thermionic emission). The higher defect density at grain boundaries is supposed to play a crucial role in the degradation of HfO$_2$ under electrical stress, which is associated with defect generation via Hf-O bond breaking. Experimentally, we observe the abrupt breakdown at the grains while a progressive breakdown is detected at the grain boundaries. The simulations suggest that this is due to the much higher density of pre-existing defects found at the grain boundaries, as correctly shown by the bright contours in Fig. 1 as well. At grains, very few pre-existing defects are present; the local defect generation rate is spatially uncorrelated (i.e., approximately constant throughout all the grain) and heavily dependent on the applied voltage. When the latter is sufficiently increased (above 4 V to 5 V approximately, in this case), it causes a sudden massive generation of additional stress-induced defects, which in turn causes a current increase; this increases the chance of local generation of new defects, triggering a thermal runaway mechanisms culminating in the abrupt breakdown, as reported in Fig. 3(a) (akin to the breakdown trends one would observe for thick oxides). Conversely, the presence of many pre-existing defects and segregation of defects in the vicinity towards the grain boundaries in HfO$_2$[35] cause the local permittivity to increase, which in turns decreases and redistributes the local electric field, leading to a more progressive breakdown, as reported in Fig. 3(b). Even at voltages lower than 4 V, the local generation rate is in this case higher due to the local temperature increase resulting from the TAT current through the defects. This favors the creation of defect clusters around the pre-existing defects, which then progressively contribute towards the creation of the BD spot (akin to the breakdown trends one would observe for very thin oxides). This dichotomy between abrupt and progressive breakdown phenomena is qualitatively similar to the one observed by Lombardo *et al.*[36] by means of device-level measurements on MOSFETs with SiO$_2$. Here, SiO$_2$ is predominantly amorphous (spatial distribution of defects follows the Poisson process) and characterized by a much lower average defect density than HfO$_2$. In that case, when the applied voltage is below a given critical value (approximately equal to 4 V), the generation rate is not critically high and causes a progressive increase in the number of defects, detected in constant voltage stress experiments.[35] Above a critical voltage, the increased generation rate results in massive defect generation, which triggers the thermal runaway and culminates in the abrupt breakdown. This picture is also consistent with previous studies on device-level time-dependent dielectric breakdown in HfO$_2$ that showed that the effective activation energy for defect generation is lower in oxygen-deficient HfO$_2$ stacks,[37] in-line with the different degradation dynamics observed on grains and grain boundaries. This difference is properly considered in our simulations by adopting different values for the activation energy at grains, $E_{A,G} = 2.8$ eV, and at grain boundaries, $E_{A,GB} = 1.9$ eV.[37] Moreover, in HfO$_2$, when oxygen vacancy defects are generated due to bond breakage, oxygen interstitials are also created.[38] These defects are also electrically active[30,31] and must be included in simulations as they could play an important role by participating in charge trapping and de-trapping. The defect parameters considered in the simulations for both positively charged oxygen vacancies and oxygen interstitials are taken from *ab–initio* calculations[30,31] and are summarized in Table I. The *I-V* curves shown in Fig. 3 are measured on randomly selected grains and grain boundaries. While Fig. 3(a) shows the abrupt breakdown of the grains, the grain boundaries show a gradual breakdown characteristic as shown in Fig. 3(b). The dotted curves in Figs. 3(a) and 3(b) show simulated *I-V* trends with a good match to the experimental curves. Twenty simulation trials were performed (ten for each site configuration) to account for the effect of the inherent variability among different grains/grain boundaries. At each trial, the position

TABLE I. Atomistic parameters of defect species taken from *ab-initio* calculations.[28,31–33]

Defect	Symbol	Thermal Ionization Energy (eV)	Relaxation Energy (eV)	Capture cross-section (cm^{-2})	Density at Grains (cm^{-3})	Density at Grain Boundaries (cm^{-3})
Positive Oxygen Vacancy	Vo$^+$	2.1±0.4	1.19±0.3	1×10^{-14}	from 3.0×10^{19}–5.0×10^{19}	from 7.0×10^{20}–9.0×10^{20}
Neutral Oxygen Interstitial	O	2.3±0.3	2.67±0.4	3.0×10^{-16}	from 1.0×10^{19}–3.0×10^{19}	from 6.0×10^{20}–7.0×10^{20}

and energy of pre-existing defects were randomly selected using a Monte-Carlo approach. Simulations accurately reproduce both the voltage dependence and the statistical variations of the currents measured on grains and GBs, together with the different breakdown dynamics.

B. Random telegraph noise at the nanoscale

Random telegraph noise (RTN), which consists of random stochastic switching of the current tunneling through a dielectric among a finite number of discrete current levels, recently gained attention due to its high relative impact on the performance and variability of ultra-scaled nanodevices. Typically, RTN is attributed to some charge trapping events at specific defect locations and is usually detected by means of standard device-level measurement techniques.[39,40] In the simplest scenario, RTN shows only two well-defined discrete current levels, which is associated with capture/emission events at a single defect.[39,41] Nevertheless, the dimensions of actual devices and the typical defect density in as-processed stacks result in a larger number of defects that may simultaneously contribute to the RTN, resulting in complex multi-level RTN trends that are computationally more involved to decode and analyze.[41] Device-level measurements are more likely to reveal RTN signals related to simultaneous capture/emission events occurring at different trap sites in the devices, hindering an accurate analysis of the experimental RTN trace of localized sites. Conversely, STM-based RTN measurements can achieve good spatial localization, potentially allowing the analysis of the behavior of individual or localized defects, especially if measurements are taken on locations that are associated with a low defect density. Studying the response of individual or localized defects would be highly beneficial when trying to understand the physical mechanisms responsible for the RTN, which are still under debate.[42–44] To address this point, we perform STM-based RTN measurements by precisely positioning the

tip on top of the grain and monitoring the current over time. Figure 4 shows the results of some of the RTN measurements at various applied bias conditions on different randomly selected grains. The RTN signals show a typical two level current fluctuation for all the bias voltages. Even though the set point voltages range between 3.5 V and 3.7 V, the actual voltage drop across the HfO$_2$ layer is very small (~19% of the applied voltage, as calculated using the Gauss Law).[15] Even though there are variations in the base level current, most of the measurements yielded current-time traces showing a two-level RTN signal, with $\frac{\Delta I}{I} \sim 25\% - 30\%$. These RTN signals are similar to the RTN signals typically detected in device-level measurements and commonly reported in the literature. This confirms that a careful choice of the experimental conditions (i.e., measuring the RTN on low defect density zones like grains and applying a proper bias voltage for a relatively short time duration) enables the potential of STM-based RTN measurements as a valuable tool for analysis of RTN signatures originating from individual defects. This is further confirmed on a statistical basis by the analysis of the current power spectral density (PSD) plots, obtained by taking a Fourier transform of the noise
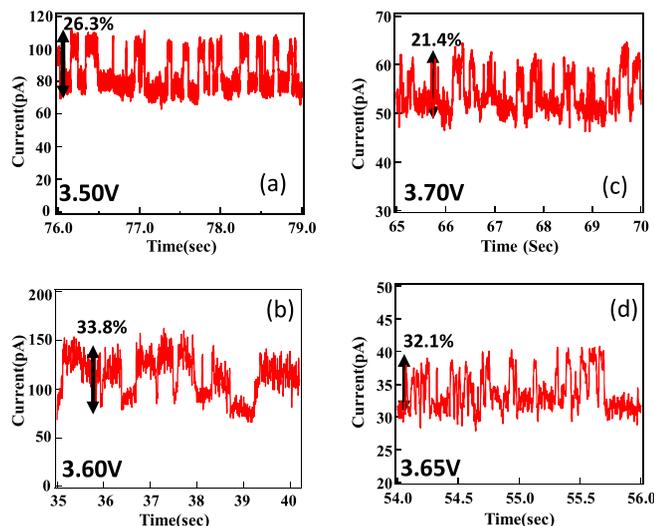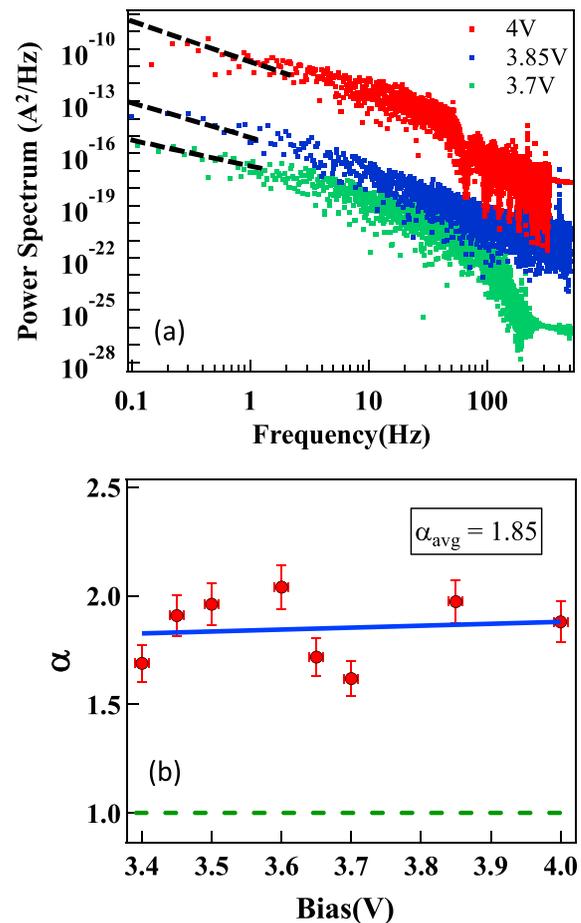

FIG. 5. (a) Power spectral density plots of the RTN signals acquired at the grain sites for three bias voltages. The low frequency regime (black dotted lines) of the spectral density plot is considered for the extraction of the power law exponent (α). For all the RTN signals measured at various bias voltages, the power law exponent is close to 1.85, as shown in (b). The green line is shown as a reference for $\alpha=1$ which corresponds to the $\frac{1}{f}$ power spectral density curve.

FIG. 4. Bias dependent random telegraph noise (RTN) signals measured of HfO$_2$ grains. The STM control voltages are also mentioned in the plots. For all the bias voltage set, a clear two-level current signal is detected. The relative amplitude of the RTN signals varies between 21% and 35% at different bias voltages.

signals at each of the applied bias voltages on different grains. The results are plotted in Fig. 5(a). The vast majority of the PSD curves have a negative slope with a value close to 2 on the log-log plot, exhibiting a Lorentzian trend (also known as $1/f^2$ noise), which corresponds to a two-level RTN fluctuation.[14] On the other hand, when many defects are being activated and deactivated, the resulting PSD curve tends to converge to a 1/f shape[15] due to the superposition of several Lorentzian curves with different time constants (roll-off points) corresponding to different physical locations and/or energy levels of multiple traps in the oxide bandgap. For the range of voltages used in our experiment, the slope (α) at low frequencies of the related PSD spectra is around 1.85 as shown in Fig. 5(b). This value is very close to the theoretical factor of 2 for pure Lorentzian behavior and the deviation is caused by the added background 1/f noise and thermal white noise contributions which always exist by default in all measurements. This shows that STM-based RTN measurements can be effectively employed to perform noise characterization at the nanoscale, focusing on individual or localized defects.

Probing RTN at the nanoscale also provides us with the possibility of gaining insights into the physical mechanisms. The latest understanding of RTN is based on the random activation and deactivation of defects, assisting charge transport, i.e., oxygen vacancies. The mechanisms responsible for activation and deactivation, though still unclear, are commonly associated with charge trapping and de-trapping at individual defects in the oxide layer.[42–44] It is typically assumed that when an individual defect participates in an electron capture/emission event, a two-level current fluctuation arises with characteristic capture/emission time constants. However, in this scenario, defects involved in RTN processes are unlikely to be the same as those involved in charge transport processes. Indeed, trapping and de-trapping at positively charged oxygen vacancies are associated with extremely small capture and emission times, which result in significant current flow.[36] Conversely, RTN capture and emission times are typically very large (on the order of milliseconds to seconds) as measured using either STM or conventional device-level techniques. This suggests that oxygen vacancy activation and deactivation may either be due to a different mechanism[44] or that trapping and de-trapping at defects of a different nature is responsible for the observed RTN.[42,43] Since the microscopic mechanisms leading to RTN are not unambiguously identified, additional efforts are required to understand the microscopic dynamics leading to such signals. From this perspective, using the STM to measure RTN increases the chances of dealing with simple patterns, which is beneficial to understand the processes involving individual defects. Moreover, due to the high spatial resolution, full 3D physics-based simulations of the entire structure of interest can be performed.

In order to reproduce the experimental RTN traces, a microscopic mechanism responsible for the activation and de-activation of the oxygen vacancy defects supporting trap-assisted tunneling should be included in the simulations.[42–44] According to a recent proposal in the literature,[42] RTN could be triggered by charge trapping at "slow" defects not directly contributing to charge transport and located in the proximity

of the ones supporting TAT (i.e., oxygen vacancies). The trapped charge perturbs the potential in its surroundings, hence changing the actual potential seen by TAT-supporting oxygen vacancy. This could temporarily inhibit the electron transport at the TAT-supporting oxygen vacancy site due to Coulomb interactions.[42] This mechanism is schematically illustrated in Fig. 6. The capture and emission processes at these defects, which were tentatively identified as oxygen interstitials,[30,42] can be described using the framework of the TAT theory. Here, we combine the potential of the localized STM-based RTN measurement with the outcomes of physics-based full-3D kinetic Monte-Carlo simulations including the effects of charge trapping and de-trapping at oxygen interstitials. Notably, the presence of this defect type was already considered when simulating the I-V curves, as the defect generation process produces defect pairs (i.e., oxygen vacancies and interstitials). Considering also charge trapping and de-trapping processes at oxygen interstitials and the Coulombic interaction between the trapped charge and the TAT-supporting oxygen vacancies strikingly allows simulations to reproduce the observed RTN. The values considered for the density of the two defect species involved (oxygen vacancies and interstitials) are the same as those used to reproduce the I-V measurements performed on grains as shown earlier in Fig. 3, which guarantees a self-consistent description of the phenomenon. The simulation results are shown in Figs. 7(a) and 7(b); note that the current range (from fractions to tens of pA), the typical relative amplitude of the current fluctuations (about 10%–20%), and the order of magnitude of the capture and emission times (from few milliseconds to several seconds) are all in good agreement with the experimental values. Moreover, the current levels and the values of $\Delta I/I$ characterizing the simulated RTN signals agree with those of the device-level[45,46] and localized observations and are consistent with activation and deactivation of individual defects.[42] Furthermore, the estimated
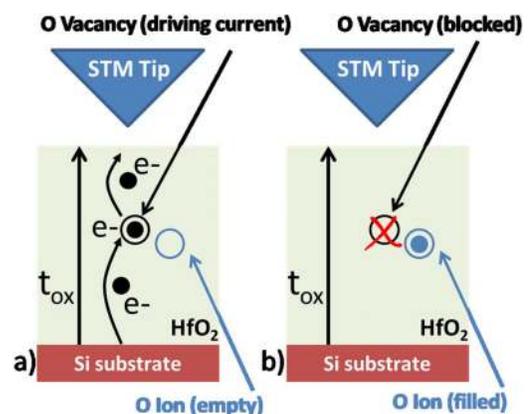

FIG. 6. Sketch of the proposed microscopic mechanism to explain measured RTN at the nanoscale. Defects in the oxide supporting trap-assisted tunneling charge transport (i.e., oxygen vacancies) can be activated (a) and deactivated (b) by charge trapping/de-trapping at additional defect species (i.e., oxygen ion). These defects are inherently slower in capturing and emitting electrons than oxygen vacancies and located in the proximity of the ones supporting charge transport. The trapped charge perturbs the potential in its surroundings, hence changing the actual potential seen by the oxygen vacancy. This could temporarily inhibit the electron transport at the oxygen vacancy due to the Coulomb interaction.
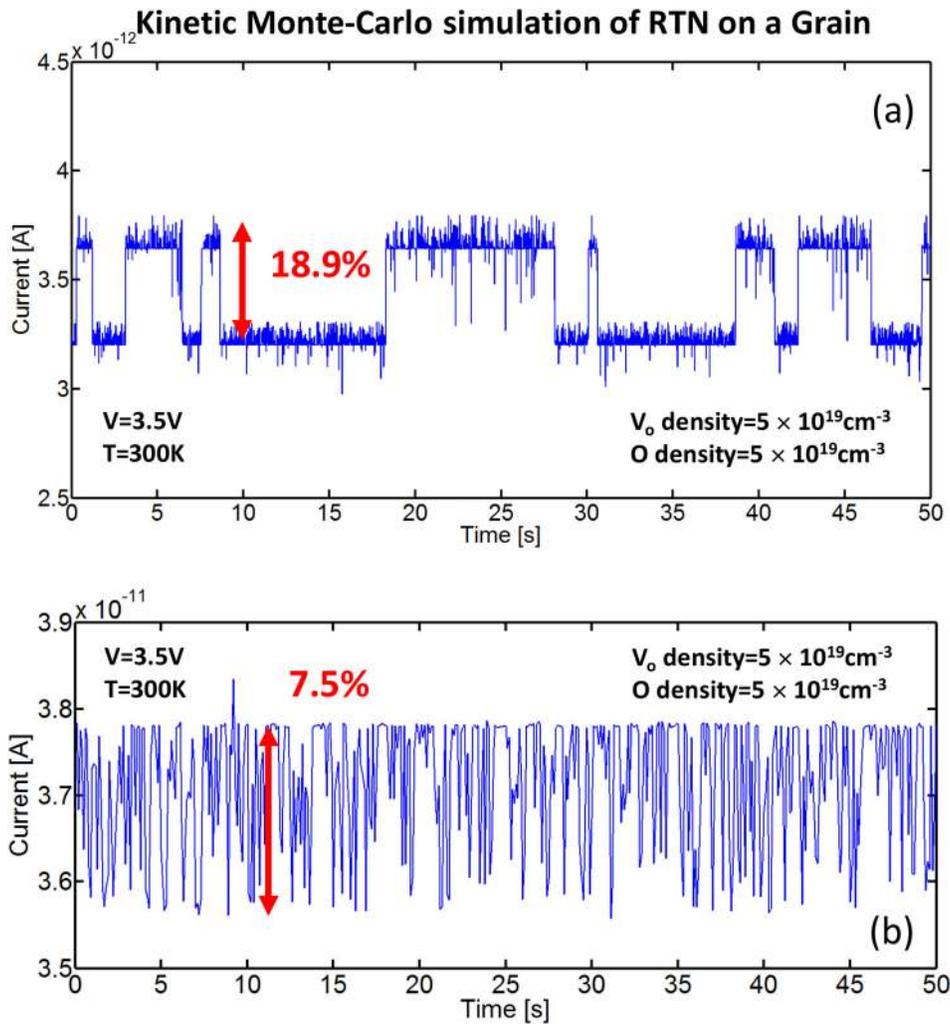
FIG. 7. Fully 3D kinetic Monte-Carlo simulations of RTN on grains. The same structure used to reproduce the *I-V* characteristics as measured on grains allows reproducing *I-t* RTN traces as measured using the STM. Considering a $10 \times 10 \, nm^2$ cell (the same size used to reproduce *I-V* curves) and the presence of oxygen vacancies/ions pairs (with the same density values used to reproduce *I-V* curves) allows approximately reproducing the characteristics of the measured RTN signals, i.e., the current range (from fractions to tens of pA), the typical relative amplitude of the current fluctuations (about 10%–20%), and the orders of magnitude of the capture and emission times (from few milliseconds to several seconds). The voltage and temperature considered in simulations are consistent with those applied in the experiments, i.e., $T = 300 \, K$ and $V = 3.5 \, V$. Notably, the simulations can also reproduce the superimposed extra noise. (a) and (b) Simulations of the RTN on different grains (simulated by randomly choosing the position and energy of the defects within the bandgap) correctly account for the inherent grain-to-grain variability of the average current and of the RTN characteristics.

density of RTN-inducing defects (i.e., oxygen interstitials $\sim10^{19} \, cm^{-3}$), together with the very small volume investigated by the STM, results in a very limited number of oxygen interstitial defects available in the structure (less than 10). Due to their random location in the oxide, only a fraction of these defects will have the right characteristics to cause RTN.[45–49] This demonstrates how the STM-based RTN measurements could be effectively used to study the characteristics of individual defects at the nanoscale. Coupling the STM technique with physics-based simulations paves the way for a refined understanding of RTN dynamics, without the complex statistical and signal processing algorithms that are typically required when dealing with more complex device-level RTN traces.[42]

IV. CONCLUSIONS

In this work, we investigated both charge transport and RTN at the nanoscale in HfO_2 using room temperature Scanning Tunneling Microscopy. The STM technique allowed the identification of grains and grain boundaries, which showed different charge transport properties. The defects responsible for charge transport in grains and grain boundaries were identified as positively charged oxygen vacancies by comparing the measured localized *I-V* curves with the predictions of a refined physics-based fully 3D

model. Furthermore, the STM technique was used to acquire RTN traces at grain locations, demonstrating the ability of this technique to investigate the properties of individual/localized defects, with a significant advantage over conventional device-level measurements. The spatially localized STM-based RTN measurements, showing the activity of individual defects, were also accurately reproduced by employing the same physical framework used to simulate the *I-V* characteristics at grains and grain boundaries. The results suggest that charge trapping at defects not directly involved in charge transport (possibly oxygen interstitials) may induce RTN through coulombic interactions with TAT-supporting defects.

[1] S. Guha and V. Narayanan, "High-κ/metal gate science and technology," Annu. Rev. Mater. Res. **39**, 181–202 (2009).

[2] B. Govoreanu, G. S. Kar, Y. Y. Chen, V. Paraschiv, S. Kubicek, A. Fantini, I. P. Radu *et al.*, "10 nm $\times$ 10 nm 2 Hf/HfOx crossbar resistive RAM with excellent performance, reliability and low-energy operation,"

in *Proceedings of the IEEE International Electron Devices Meeting (IEDM)* (IEEE, 2011), pp. 313–316.

[3]J. Robertson, "High dielectric constant oxides," Eur. Phys. J. Appl. Phys. **28**(03), 265–291 (2004).

[4]F. Crupi, R. Degraeve, A. Kerber, D. H. Kwak, and G. Groeseneken, "Correlation between stress-induced leakage current (SILC) and the HfO_2 bulk trap density in a SiO_2/HfO_2 stack," in *Proceedings of the 42nd Annual International Reliability Physics Symposium* (IEEE, 2004), pp. 181–187.

[5]A. Neugroschel, G. Bersuker, R. Choi, C. Cochrane, P. Lenahan, D. Heh, and R. Jammy, "An accurate lifetime analysis methodology incorporating governing NBTI mechanisms in high-k/SiO_2 gate stacks," in *Proceedings of the International Electron Devices Meeting(IEDM)* (IEEE, 2006), pp. 1–4.

[6]E. Cartier, B. P. Linder, V. Narayanan, and V. K. Paruchuri, "Fundamental understanding and optimization of PBTI in nFETs with SiO_2/HfO_2 gate stack," in *Proceedings of the International Electron Devices Meeting* (IEEE, 2006), pp. 1–4.

[7]Y. T. Chung, Y. H. Liu, P. C. Su, Y. H. Cheng, T. Wang, and M. C. Chen, "Investigation of random telegraph noise amplitudes in hafnium oxide resistive memory devices," in *Proceedings of the IEEE International Reliability Physics Symposium* (IEEE, 2014), p. MYM–2.

[8]Y. H. Kim and J. C. Lee, "Reliability characteristics of high-κ dielectrics," Microelectron. Reliab. **44**(2), 183–193 (2004).

[9]N. Raghavan, K. L. Pey, and K. Shubhakar, "High-κ dielectric breakdown in nanoscale logic devices–scientific insight and technology impact," Microelectron. Reliab. **54**(5), 847–860 (2014).

[10]X. Wu, D. B. Migas, X. Li, M. Bosman, N. Raghavan, V. E. Borisenko, and K. L. Pey, "Role of oxygen vacancies in HfO_2-based gate stack breakdown," Appl. Phys. Lett. **96**(17), 172901 (2010).

[11]G. Bersuker, D. Heh, C. Young, H. Park, P. Khanal, L. Larcher, and H. Tseng, "Breakdown in the metal/high-κ gate stack: Identifying the "weak link" in the multilayer dielectric," IEEE Int. Electron Dev. Meet. 791–794 (2008).

[12]H. D. Xiong, D. Heh, S. Yang, X. Zhu, M. Gurfinkel, G. Bersuker, and J. S. Suehle, "Stress-induced defect generation in HfO_2/SiO_2 stacks observed by using charge pumping and low frequency noise measurements," in *Proceedings of the Reliability Physics Symposium (IRPS)* (IEEE, 2008), pp. 319–323.

[13]J. P. Campbell, J. Qin, K. P. Cheung, L. C. Yu, J. S. Suehle, A. Oates, and K. Sheng, "Random telegraph noise in highly scaled nMOSFETs," in *Proceedings of the International Reliability Physics Symposium* (IEEE, 2009), pp. 382–388.

[14]W. H. Liu, K. L. Pey, N. Raghavan, X. Wu, and M. Bosman, "Triggering voltage for post-breakdown random telegraph noise in HfLaO dielectric metal gate metal-oxide semiconductor field effect transistors and its reliability implications," J. Appl. Phys. **111**, 024101 (2012).

[15]R. Thamankar, N. Raghavan, J. Molina, F. M. Puglisi, S. J. O'Shea, K. Shubhakar, L. Larcher, P. Pavan, A. Padovani, and K. L. Pey, "Single vacancy defect spectroscopy on HfO_2 using random telegraph noise signals from scanning tunneling microscopy," J. Appl. Phys. **119**, 084304 (2016).

[16]M. Lanza, G. Bersuker, M. Porti, E. Miranda, M. Nafría, and X. Aymerich, "Resistive switching in hafnium dioxide layers: Local phenomenon at grain boundaries," Appl. Phys. Lett. **101**, 193502 (2012).

[17]M. Lanza, K. Zhang, M. Porti, M. Nafria, Z. Y. Shen, L. F. Liu, J. F. Kang, D. Gilmer, and G. Bersuker, "Grain boundaries as preferential sites for resistive switching in the HfO2 resistive random access memory structures," Appl. Phys. Lett. **100**, 123508 (2012).

[18]F. M. Puglisi, U. Celano, A. Padovani, W. Vandervorst, L. Larcher, and P. Pavan, "Scaling perspective and reliability of conductive filament formation in ultra-scaled HfO_2 resistive random access Memory," in *Proceedings of the IEEE International Reliability Physics Symposium (IRPS)* (2017), pp. PM-8.1–PM-8.5.

[19]U. Celano, T. Hantschel1, G. Giammaria, R. C. Chintala, T. Conard, H. Bender, and W. Vandervorst, "Evaluation of the electrical contact area in contact mode scanning probe microscopy," J. Appl. Phys. **117**(21), 214305 (2015).

[20]Y. L. Chen, J. Wang, C. M. Xiong, R. F. Dou, J. Y. Yang, and J. C. Nie, "Scanning tunneling microscopy/spectroscopy studies of resistive switching in Nbdoped $SrTiO_3$," J. Appl. Phys. **112**, 023703 (2012).

[21]A. Nayak, Q. Wang, Y. Itoh, T. Tsuruoka, T. Hasegawa, L. Boodhoo, H. Mizuta, and M. Aono, "Position detection and observation of a conducting filament hidden under a top electrode in a Ta_2O_5-based atomic switch," Nanotechnology **26**, 145702 (2015).

[22]A. Nayak, T. Tamura, T. Tsuruoka, K. Terabe, S. Hosaka, T. Hasegawa, and M. Aono, "Rate-limiting processes determining the switching time in a Ag_2S atomic switch," J. Phys. Chem. Lett. **1**, 604–608 (2010).

[23]W. Anja, L. Michael, D.-Y. Cho, M. Marco, S. Katharina, R. Vikas, H. Tsuyoshi, K. K. Adepalli, B. Yildiz, R. Waser, and I. Valov, "Nanoscale cation motion TaO_x, HfO_x TiO_x memristive systems," Nat. Nanotechnol. **684**(11), 67–74 (2016).

[24]A. Mehonic, S. Cueff, M. Wojdak, S. Hudziak, C. Labbé, R. Rizk, and A. J. Kenyon, Nanotechnology **23**, 455201 (2012).

[25]M. Moors, K. K. Adepalli, Q. Lu, A. Wedig, C. Bäumer, K. Skaja, B. Arndt, H. L. Tuller, R. Dittmann, R. Waser, B. Yildiz, and I. Valov, "Resistive switching mechanisms on TaO_x and $SrRuO_3$ thin-film surfaces probed by scanning tunneling microscopy," ACS Nano **10**(1), 1481–1492 (2016).

[26]T. Ando, "Ultimate scaling of high-κ gate dielectrics: Higher-κ or interfacial layer scavenging?," Materials **5**(3), 478–500 (2012).

[27]O. Pirrotta, L. Larcher, M. Lanza, A. Padovani, M. Porti, M. Nafría, and G. Bersuker, "Leakage current through the poly-crystalline HfO_2: Trap densities at grains and grain boundaries," J. Appl. Phys. **114**(13), 134503 (2013).

[28]F. Puglisi, L. Larcher, A. Padovani, and P. Pavan, "Operations, charge transport, and random telegraph noise in HfO_x resistive random-access memory: A multi-scale modeling study," MRS Adv. **1**(5), 327–338 (2016).

[29]L. Larcher, A. Padovani, and L. Vandelli, "A simulation framework for modeling charge transport and degradation in high-k stacks," J. Comput. Electron. **12**(4), 658–665 (2013).

[30]D. Muñoz Ramo *et al.*, "Spectroscopic properties of oxygen vacancies in monoclinic HfO_2 calculated with periodic and embedded cluster density functional theory," Phys. Rev. B **75**, 205336 (2007).

[31]A. S. Foster *et al.*, "Vacancy and interstitial defects in Hafnia," Phys. Rev. B: Condens. Matter **65**(17), 174117 (2002).

[32]J. W. McPherson, J. Kim, A. Shanware, H. Mogul, and J. Rodriguez, "Trends in the ultimate breakdown strength of high dielectric-constant materials," IEEE Trans. Electron Devices **50**(8), 1771–1778 (2003).

[33]K. Shubhakar, K. L. Pey, N. Raghavan, S. S. Kushvaha, M. Bosman, Z. Wang, and S. J. O'Shea, "Study of preferential localized degradation and breakdown of HfO_2/SiO_x dielectric stacks at grain boundary sites of polycrystalline HfO_2 dielectrics," Microelectron. Eng. **109**, 364–369 (2013).

[34]M. Lanza, V. Iglesias, M. Porti, M. Nafria, and X. Aymerich, "Polycrystallization effects on the nanoscale electrical properties of high-k dielectrics," Nanoscale Res. Lett. **6**, 108 (2011).

[35]K. McKenna and A. Shluger, "The interaction of oxygen vacancies with grain boundaries in monoclinic HfO_2," Appl. Phys. Lett. **95**, 222111 (2009).

[36]S. Lombardo, J. H. Stathis, and B. P. Linder, "Breakdown transients in ultrathin gate oxides: Transition in the degradation rate," Phys. Rev. Lett. **90**, 167601 (2003).

[37]A. Padovani, L. Larcher, G. Bersuker, and P. Pavan, "Charge transport and degradation in HfO_2 and HfO_x dielectrics," IEEE Electron Device Lett. **34**(5), 680–682 (2013).

[38]J. McPherson, J.-Y. Kim, A. Shanware, and H. Mogul, "Thermochemical description of dielectric breakdown in high dielectric constant materials," Appl. Phys. Lett. **82**, 2121–2123 (2003).

[39]H. Miki, N. Tega, M. Yamaoka, D. J. Frank, A. Bansal, M. Kobayashi *et al.*, "Statistical measurement of random telegraph noise and its impact in scaled-down high-κ/metal-gate MOSFETs," in *Proceedings of the IEEE International Electron Devices Meeting (IEDM)* (IEEE, 2012), p. 1.

[40]M. J. Uren, D. J. Day, and M. Kirton, "1/f and random telegraph noise in silicon metal-oxide-semiconductor field-effect transistors," Appl. Phys. Lett. **47**(11), 1195–1197 (1985).

[41]F. M. Puglisi and P. Pavan, "Factorial hidden Markov model analysis of random telegraph noise in resistive random access memories," ECTI Trans. Electr. Eng., Electron., Commun. **12**(1), 24–29 (2014).

[42]F. M. Puglisi *et al.*, "A microscopic physical description of RTN current fluctuations in HfO_x RRAM," in *Proceedings of the IEEE International Reliability Physics Symposium (IRPS)*, Monterey, CA, 19–23 April 2015, pp. 5B.5.1-5B.5.6.

[43]F. M. Puglisi, L. Larcher, A. Padovani, and P. Pavan, "A complete statistical investigation of RTN in HfO_2-based RRAM in high resistive state," IEEE Trans. Electron Devices **62**(8), 2606–2613 (2015).

[44]T. Grasser, "Stochastic charge trapping in oxides: From random telegraph noise to bias temperature instabilities," Microelectron. Reliab. **52**, 39–70 (2012).

[45]H.-J. Cho, S. Lee, B.-G. Park, and H. Shin, "Extraction of trap energy and location from random telegraph noise in gate leakage current (Ig RTN) of metal–oxide semiconductor field effect transistor (MOSFET)," Solid-State Electron. **54**, 362–367 (2010).

[46]H.-J. Cho, Y. Son, B.-C. Oh, S. Lee, J.-H. Lee, B.-G. Park, and H. Shin, "Study on time constants of random telegraph noise in gate leakage current through hot-carrier stress test," IEEE Electron Devices Lett. **31**(9), 1029 (2010).

[47]F. Puglisi and P. Pavan, "RTN analysis with FHMM as a tool for multi-trap characterization in HfO_x RRAM," in *Proceedings of the IEEe International Conference of Electron Devices and Solid-State Circuits (EDSSC)* (IEEE, 2013), pp. 1–2.

[48]F. M. Puglisi, P. Pavan, A. Padovani, L. Larcher, and G. Bersuker, "RTS noise characterization of HfO_x RRAM in high resistive state," Solid-State Electron. **84**, 160–166 (2013).

[49]F. M. Puglisi, P. Pavan, A. Padovani, and L. Larcher, "A study on HfO_2 RRAM in HRS based on I–V and RTN analysis," Solid-State Electron. **102**, 69–75 (2014).